THE JOURNAL OF BIOLOGICAL CHEMISTRY VOL. 291, NO. 14, pp. 7754–7766, April 1, 2016

Increased Energy Expenditure, *Ucp1* Expression, and Resistance to Diet-induced Obesity in Mice Lacking Nuclear Factor-Erythroid-2-related Transcription Factor-2 (*Nrf2*)*

Received for publication, June 22, 2015, and in revised form, February 1, 2016 Published, JBC Papers in Press, February 3, 2016, DOI 10.1074/jbc.M115.673756

Kevin Schneider[‡], Joshua Valdez[‡], Janice Nguyen[‡], Marquis Vawter[§], Brandi Galke[§], Theodore W. Kurtz[¶], and Jefferson Y. Chan[‡1]

From the [‡]Department of Laboratory Medicine and Pathology and the [§]Department of Psychiatry and Human Behavior, University of California, Irvine, California 92697 and the [¶]Department of Laboratory Medicine, University of California, San Francisco, California 94107

The NRF2 (also known as NFE2L2) transcription factor is a critical regulator of genes involved in defense against oxidative stress. Previous studies suggest that *Nrf2* plays a role in adipogenesis *in vitro*, and deletion of the *Nrf2* gene protects against diet-induced obesity in mice. Here, we demonstrate that resistance to diet-induced obesity in *Nrf2*$^{-/-}$ mice is associated with a 20–30% increase in energy expenditure. Analysis of bioenergetics revealed that *Nrf2*$^{-/-}$ white adipose tissues exhibit greater oxygen consumption. White adipose tissue showed a >2-fold increase in *Ucp1* gene expression. Oxygen consumption is also increased nearly 2.5-fold in *Nrf2*-deficient fibroblasts. Oxidative stress induced by glucose oxidase resulted in increased *Ucp1* expression. Conversely, antioxidant chemicals (such as *N*-acetylcysteine and Mn(III)tetrakis(4-benzoic acid) porphyrin chloride) and SB203580 (a known suppressor of *Ucp1* expression) decreased *Ucp1* and oxygen consumption in *Nrf2*-deficient fibroblasts. These findings suggest that increasing oxidative stress by limiting *Nrf2* function in white adipocytes may be a novel means to modulate energy balance as a treatment of obesity and related clinical disorders.

Obesity is characterized by excess adipose tissue mass, and it is associated with various chronic diseases, including type 2 diabetes, hypertension, atherosclerosis, and cancer. Obesity is currently one of the leading causes of morbidity and mortality globally. There are two different types of adipose tissues in mammals: white adipose tissue and brown adipose tissue. White adipose tissue (WAT)[2] serves an important role in maintaining energy homeostasis in the body by storing surplus energy as triglyceride and releasing free fatty acids to meet the needs of other organs when energy intake is less than energy expenditure. White adipocytes contain few mitochondria and are characterized by a single, large lipid droplet. Brown adipose tissue (BAT) is specialized in energy consumption through heat production in response to cold or excess calories. This response, known as adaptive thermogenesis, protects against cold exposure and plays a beneficial role in regulating energy balance in mice that have a variable diet (1, 2). Brown adipocytes contain multiple small lipid droplets and are highly enriched in mitochondria. In humans, BAT is abundant in newborns, and it was originally thought to be nonexistent or nonfunctional in adults. However, recent studies have shown metabolically active BAT in adult humans through the use of PET/CT scans (positron emission tomography associated with computed tomography) (3–5). These BAT depots are observed in the neck and in other locations, including the suprarenal, supraclavicular, and paravertebral region of the body (6–11).

The thermogenic function of BAT is dependent on UCP1, a protein expressed in the inner mitochondrial membrane of brown fat cells that functions to dissipate the proton gradient generated during oxidative phosphorylation. This is achieved by increasing the permeability of the inner mitochondrial membrane, allowing protons that have been pumped into the intermembrane space to return to the mitochondrial matrix. This proton leak, termed mitochondrial uncoupling, is physiologically relevant, accounting for 20–25% of the basal metabolic rate (12–14). Studies have shown that mice lacking *Ucp1* are more susceptible to diet-induced obesity (15). Conversely, transgenic mice with increased *Ucp1* expression in WAT are resistant to high fat diet-induced obesity (16). In addition, transgenic mice expressing *Ucp1* in skeletal muscle showed improved glucose tolerance after being fed a high fat diet when compared with wild type mice (17). In humans, it has been estimated that as little as 50 g of BAT (<0.1% of body weight) could utilize up to 20% of basal caloric needs if maximally stimulated (2). Because of the enormous thermogenic capacity of BAT, there has been intense interest in the determinants of BAT function and the potential for treating obesity by manipulating BAT function. In addition to brown adipose tissue, several studies have shown that brown-like adipocytes (often referred to as "brite" or "beige" adipocytes) occur in some classical white adipose depots as well as skeletal muscle and that these serve as extremely promising targets for treatment of obesity (18–21).

* This work was supported in part by National Institute of Health Research Grant CA091907 to J. Y. C. The authors declare that they have no conflicts of interest with the contents of this article.

[1] To whom correspondence should be addressed: Dept. of Laboratory Medicine and Pathology, University of California, Irvine, D440 Medical Science 1, Irvine, CA 92697. E-mail: jchan@uci.edu.

[2] The abbreviations used are: WAT, white adipose tissue(s); BAT, brown adipose tissue; CM-H2DCFDA, chloromethyl-2′,7′-dichlorodihydrofluorescein diacetate; BHA, butylated hydroxyanisole; MaTBAP, Mn(III)tetrakis(4-benzoic acid)porphyrin chloride; MEF, mouse embryo fibroblast; OCR, oxygen consumption rate; FCCP, carbonyl cyanide-*p*-trifluoromethoxyphenylhydrazone; ANOVA, analysis of variance; RNA-seq, RNA sequencing.

NRF2 (nuclear factor-erythroid 2-related factor 2, also known as NFE2L2) is a member of the Cap-N-Collar subfamily of bZIP transcription factors that also includes NRF1, p45NFE2, and NRF3 (22–24). Under basal conditions, NRF2 is maintained at low levels through the ubiquitin proteasome proteolytic pathway mediated by KEAP1 (Kelch-like ECH-associated protein 1) (24, 25). In response to oxidative stress, NRF2 escapes KEAP1-mediated negative regulation, resulting in nuclear accumulation of NRF2 (26). NRF2 is able to form heterodimers with other transcription factors, including sMAF (small Maf proteins), JUND, and ATF4 (activation transcription factor 4), to bind and activate gene transcription via cis-acting antioxidant response elements in the promoters of cellular defense genes (27–30). These genes include a wide variety of enzymes involved in detoxification, such as NAD(P)H quinone oxidoreductase 1 and heme oxygenase 1 (31, 32). *Nrf2* is also involved in driving the expression of key antioxidant enzymes, such as the catalytic and regulatory subunits of γ-glutamate cysteine ligase, and phase 2 enzymes, such as glutathione transferases (33). Mice lacking the *Nrf2* gene demonstrate no obvious outward defects; however, they have an increased susceptibility to toxicant and oxidative stress-induced diseases, and they are also more prone to developing autoimmune disorders as they age (34–38). Compared with wild type mice, *Nrf2* mutant mice have also been shown to be more sensitive to carcinogens in the stomach, suggesting an important role of *Nrf2* and antioxidant response in the protection against cancer (39).

Recent findings suggest that *Nrf2* plays a role in regulating the expression of key genes involved in the process of adipogenesis (40, 41). In addition, mice lacking *Nrf2* demonstrate a resistance to high fat diet-induced obesity, but the underlying mechanism is not clear (41). In this study, we explored the role of *Nrf2* in mitochondrial function. Specifically, we assessed energy expenditure, changes in adipose tissue mass, morphology, and gene expression in $Nrf2^{-/-}$ mice fed both a normal and high fat diet. In addition, $Nrf2^{-/-}$ cells were assessed for mitochondrial function and gene expression. Our studies are consistent with the hypothesis that oxidative stress modulates mitochondrial function to control fat storage and energy expenditure in *Nrf2* knock-outs.

Experimental Procedures

Reagents—Dulbecco's modified Eagle's medium (DMEM), α-minimum essential medium, fetal bovine serum (FBS), L-glutamine, penicillin, streptomycin, CM-H2DCFDA, MitoTracker Green FM, nanoyl-acridine orange, and Superscript III reverse transcriptase were purchased from Invitrogen. Glucose oxidase, butylated hydroxyanisole (BHA), and anti-β-actin antibody (A1978) were purchased from Sigma. UCP1 (ab23841) antibody was purchased from Abcam (Cambridge, MA). α-Tubulin antibody (ab3873) was purchased from Cell Signaling (Beverly, MA). TRIzol RNA reagent, 2× FastStart SYBR Green Master mix, was purchased from Roche Applied Science. The RNeasy MinElute cleanup kit was from Qiagen (Valencia, CA). The enhanced chemiluminescence substrate kit was from Pierce. Mn(III)tetrakis(4-benzoic acid)porphyrin chloride (MnTBAP) was purchased from EMD Millipore (Billerica, MA).

Cells—Mouse embryonic fibroblasts (MEFs) were generated as described previously (41) and cultured in DMEM supplemented with 10% FBS, 8.3 mM L-glutamine, 100 units/ml penicillin, and 100 μg/ml streptomycin. Oxidative stress was induced in cells by incubating with 25 milliunits/ml glucose oxidase for 6 h at 37 °C, and antioxidant treatment was accomplished by incubation with 40 μM BHA or with 10 μM MnTBAP.

Mice—All experiments were carried out following guidelines of the University of California Irvine institutional animal care and use committee. *Nrf2* knock-out mice have been described previously (42) and were back-crossed 10 generations to C57BL/6J background to produce nearly isogenic lines. Studies were done using age-matched 12–16-week-old $Nrf2^{-/-}$ and wild type male mice. Mice were housed on 12-h light and dark cycles under controlled environmental settings (23 ± 1 °C), with free access to food and water. Age-matched wild type and $Nrf2^{-/-}$ mice were fed either a standard global rodent diet (Harland Teklad 2020x) or a high fat diet chow containing 60% kcal from fat (Harlan Teklad TD.06414). The fatty acid profile of the high fat diet as a percentage of total fat consists of 37% saturated, 47% monounsaturated, of 16% polyunsaturated fat.

Metabolic and Indirect Calorimetry Studies—Indirect calorimetry to measure oxygen (O_2) consumption, carbon dioxide (CO_2) production, activity, and food intake was done using the Comprehensive Laboratory Animal Monitoring System (Columbus Instruments, Columbus, OH). Mice were individually housed in metabolic chambers maintained at 20–22 °C in a 12-h light/12-h dark cycle. After the mice had adapted to the environment of the metabolic chamber for 72 h, metabolic parameters were assessed. Activity was monitored by the number of times a mouse moved through infrared beams crossing the cages. Body fat and lean mass were measured using an EchoMRI-100 (Echo Medical Systems, Houston, TX). Glucose tolerance tests were conducted in animals that were fasted overnight. Glucose was administered by intraperitoneal injection at a dose of 1 mg/g body weight. Blood samples were collected from the tail vein at time 0 (prior to the glucose injection) and 30, 60, and 120 min after glucose loading for blood glucose. Blood glucose concentrations were measured using a TRUETest blood glucose meter (Nipro Diagnostics, Fort Lauderdale, FL). Fasting serum triglyceride levels were analyzed with a serum triglyceride kit according to the manufacturer's instructions (Sigma), and serum concentrations of insulin were determined using the Ultra Sensitive Mouse Insulin ELISA Kit from Crystal Chem (Downers Grove, IL).

RNA Isolation and Quantitative Real-time PCR—RNA was extracted using TRIzol RNA reagent and further purified using the RNeasy MinElute Cleanup Kit. cDNA synthesis was generated with a Superscript III first-strand synthesis kit according to the manufacturer's recommendation. Amplification of cDNA occurred in a Step One Plus PCR machine (ABI) using the FastStart SYBR Green reagent in duplicate 10-μl reactions. The ribosomal phosphoprotein large P0 (RPLP0) gene was used as a reference control, and relative expression was calculated using the expression, $2^{(Ct\ \text{test gene}\ -\ Ct\text{RPLP}^0)}$. -Fold change in expression was determined from the difference between the averaged expression levels relative to control. Primers used are listed in Table 1.

TABLE 1
List of primers

Gene	Forward	Reverse
Pgc1α	CGGAAATCATATCCAACCAG	TGAGGACCGCTAGCAAGTTTG
NRF1	CGCAGCACCTTTGGAGAA	CCCGACCTGTGGAATACTTG
Dio2	AAGCACGTGGCGTTGCTTCTG	TGGAGACGTGCACCACACTGG
Ucp1	ACTGCCACACCTCCAGTCATT	CTTTGCCTCACTCAGGATTGG
Cox7a1	GGGCGAAGAGGGGAGGTGAC	TTGTCCATTCCCCCGCCTTT
Cox8b	GAACCATGAAGCCAACGACT	GCGAAGTTCACAGTGGTTCC
Sirt3	TGGCGTTGTGAAACCCGACA	AACGAACGGCCCCACCAAGT
CideA	TGCTCTTCTGTATCGCCAGT	GCCGTGTTAAGGAATCTGCTG
Tfam	GGAATGTGGAGCGTGCTAAAA	TGCTGGAAAACACTTCGGAATA
Rplpo	CCCCTTCTCCTTCGGGCTGAT	GTGTGGCACCGAGGCAACAGT

Western Blotting—Protein lysates were prepared using Nonidet P-40 lysis buffer, and protein concentrations were determined using Bio-Rad protein assay reagent with BSA as the protein standard. Samples were electrophoresed on SDS-polyacrylamide gels and transferred onto nitrocellulose membranes. Membranes were then blocked in 5% milk at room temperature for 1 h and incubated with primary antibody overnight at 4 °C. Subsequently, blots were washed, and peroxidase-conjugated secondary antibody was added and incubated for 1 h. Blots were visualized using a chemiluminescent detection system.

Histology and Immunohistochemistry—Tissues were fixed in 10% neutral buffered formalin and imbedded in paraffin. Tissue sections were stained with H&E and visualized using a Nikon microscope equipped with a CCD camera.

RNA Sequencing (RNA-seq) Analysis—From WAT of mice fed a high fat diet, total RNA was isolated using TRIzol RNA reagent and further purified using RNeasy MinElute Cleanup Kit. Three independent replicates were used for both wild type and $Nrf2^{-/-}$ mice. Integrity and purity of the samples were assessed using an Agilent Bioanalyzer, and libraries for RNA-Seq were generated using the Illumina Truseq kit version 2 per the manufacturer's instructions. RNA-seq libraries were sequenced on an Illumina HiSeq 2500 next generation sequencer using single read 50-bp (SR50) chemistry with a read depth of >10 million reads/sample. Reads are processed and mapped to a reference genome (mm10, built name NCBIM37) using ELAND. Transcript abundance quantification was assigned using normalized read counts, such as FPKM, and statistical testing for differential expression was performed using Cufflinks. Differentially expressed genes were further analyzed using Ingenuity Pathways Analysis.

Flow Cytometry—For intracellular reactive oxygen species measurements, cells were incubated with 10 μM CM-H2DCFDA in PBS for 15 min at 37 °C. Fluorescence was analyzed by flow cytometry. Oxidative stress was induced in cells by incubating with 25 milliunits/ml glucose oxidase for 6 h at 37 °C prior to CM-H2DCFDA staining. Antioxidant treatment was accomplished by incubation with 100 μM BHA for 6 h at 37 °C.

Measurement of Oxygen Consumption in Adipocytes and MEF Cells Using the XF24 Extracellular Flux Analyzer—The Seahorse XF24 Extracellular Flux Analyzer was utilized for measuring the oxygen consumption of adherent MEF cells as well as extracted adipose tissue explants. The protocol for acquisition of intra-abdominal WAT, preparation of tissue, and usage of XF24 was performed as described previously (43), with minor changes. The sensor cartridge was calibrated with calibration buffer (Seahorse Bioscience, North Billerica, MA) at 37 °C the day before oxygen consumption rate (OCR) measurements. Intra-abdominal WAT was dissected into small pieces (~5 mg) and washed extensively with XF-Basal Medium containing 25 mM HEPES and 25 mM glucose. Two pieces of isolated WAT weighing a total of 10 mg were placed into each well of a XF24 Islet Capture Microplate (Seahorse Bioscience), and each well was covered with a capture screen to hold the tissues in place while allowing for free perfusion. XF Basal Medium supplemented with 25 mM glucose, 1 mM sodium pyruvate, and 2 mM L-glutamine (450 μl) was then added, and the OCR was measured in a XF24 extracellular flux analyzer (Seahorse Bioscience) according to the manufacturer's protocol. OCR readings were taken over time under basal conditions and after the addition of mitochondrial inhibitors, oligomycin (8 μg/ml), carbonyl cyanide-*p*-trifluoromethoxyphenylhydrazone (FCCP; 8 μM), and a mixture of rotenone (3 μM) and antimycin-A (12 μM), in succession. A minimum of five wells were utilized per condition in any given experiment. Plates were saved, and tissue protein concentrations were measured by a Bradford assay. OCR was determined by Seahorse XF-24 software as a function of time and normalized by protein concentration (pmol/min/μg), respectively. Bioenergetic parameters assessed were basal, ATP-linked respiration, proton leak, maximal, and reserve capacity. The basal respiration rate was calculated by subtracting the residual OCR determined after the addition of rotenone and antimycin-A. ATP-linked respiration was determined from the difference between basal OCR and OCR following oligomycin addition. The difference in OCR between rotenone and oligomycin represented the amount of oxygen consumed that is due to proton leak. Maximal OCR was determined by subtracting the OCR after rotenone addition from the OCR induced by FCCP. Last, the reserve capacity was calculated by the difference between maximal and basal respiration. All data are expressed as a percentage of the basal OCR to allow comparison between the different genotypes. For MEF cells, 50,000 cells were plated in XF 24-well plates 1 day before analysis. This allowed for 70–90% confluence on the day of measurement. The sensor cartridge was hydrated 24 h before the run as indicated by the manufacturer's protocol. On the day of the run, cells were washed two times with Seahorse Basal Medium containing 25 mM glucose, 1 mM sodium pyruvate, and 4 mM L-glutamine and then covered with 450 μl of the same basal medium. The OCR was measured in a XF24 extracellular flux analyzer (Seahorse Bioscience) according to the manufacturer's protocol. OCR readings were taken over time under basal conditions and after the addition of mitochondrial inhibitors, oligomycin (1 μM), FCCP (1 μM), and a mixture of rotenone (1 μM) and

antimycin-A (1 μM), in succession. A minimum of five wells were utilized per condition in any given experiment. Plates were saved, and cellular protein concentrations were measured by a Bradford assay. OCR was determined by Seahorse XF-24 software as a function of time and normalized by protein concentration (pmol/min/μg), respectively.

Measurement of Oxygen Consumption Utilizing the BD Oxygen Biosensor Plate—Fluorometric measurements of oxygen consumption in adherent mouse cells were done using BD Oxygen Biosensor plates (BD Biosciences) (44). Triplicate wells were seeded with 2×10^5 cells suspended in 25 mM glucose DMEM without phenol red. Plates were scanned every 5 min for 120 min in a temperature-controlled (37 °C) plate reader (Thermo, Waltham, MA) with an excitation wavelength of 485 nm and an emission wavelength of 630 nm. Fluorescence values for each well were normalized to their initial value and then to the values of no-cell controls at each time point.

GSH and GSSG Assay—Measurements of GSH and GSSG levels were determined using the Glutathione Assay Kit (Cayman Chemical, Ann Arbor, MI) following the manufacturer's protocol. Tissues were homogenized in 5–10 ml of cold 50 mM MES buffer/g of tissue. Homogenates were spun at 10,000 $\times$ *g* for 15 min, and supernatant fractions were collected. Supernatant fractions were assayed for total reduced (GSH) and oxidized (GSSG) glutathione by the standard enzymatic recycling method after deproteination of samples using 5% metaphosphoric acid and the addition of triethanolamine. Samples for GSSG determination were first incubated at room temperature with 2 μl of 4-vinylpyridine/100-μl sample for 1 h after vigorous vortexing in order to derivatize endogenous GSH and allow for measurement of GSSG specifically. The GSSG was then subtracted from the total GSH to determine actual GSH level and GSH/GSSG ratio, which is used as an indicator for oxidative stress (45).

Statistical Analysis—Data are expressed as means ± S.E., and statistical analysis was done using GraphPad Prism (GraphPad Software, Inc., La Jolla, CA). For simple comparisons of two groups, a two-tailed Student's *t* test for unpaired samples was used. For comparisons of wild type and knock-out groups concerning the influence of high fat diet, a two-way ANOVA analysis was used, followed by a post hoc Bonferroni analysis. *p* values of ≤ 0.05 were considered statistically significant and are indicated.

Results

$Nrf2^{-/-}$ Mice Are Resistant to High Fat Diet-induced Obesity—The body weights of wild type and $Nrf2^{-/-}$ male mice were indistinguishable at 12 weeks of age when fed a standard chow diet (Fig. 1*A*). This observation in mice derived from a C57BL/6 background is consistent with our previous results in mice derived from a mixed C57BL/6 $\times$ Sv129 genetic background (41). After exposure to a high fat diet for 6 weeks, the mean body weight of $Nrf2^{-/-}$ mice was 25% less than that of wild type mice (Fig. 1*A*). Wild type mice nearly doubled their starting weight, whereas $Nrf2^{-/-}$ mice only gained 50% of their starting weight (Fig. 1*A*). A comparison of adipose tissue mass normalized to lean body mass measured by EchoMRI showed that $Nrf2^{-/-}$ mice exposed to a high fat diet had 50% less whole-body fat compared with wild type mice. Importantly, there was no significant change in the lean body mass of $Nrf2^{-/-}$ mice compared with wild type mice (Fig. 1*B*). The white and brown adipose tissue weights normalized to body weight were 30% lower in $Nrf2^{-/-}$ mice compared with wild type mice. Relative weights of liver, heart, and kidney were not different between wild type and $Nrf2^{-/-}$ mice (Fig. 1*C*) (data not shown). To rule out possible lipid deposition in other tissues, sections of various tissues were analyzed. Ectopic accumulation of lipids was not observed in heart or skeletal tissues of both wild type and $Nrf2^{-/-}$ mice placed on a high fat diet (Fig. 1*D*). However, wild type mice demonstrated significant liver steatosis compared with $Nrf2^{-/-}$ mice (Fig. 1*D*). These results indicate that lower fat mass in $Nrf2^{-/-}$ mice is not associated with increased lipid accumulation in non-adipose tissues. Along with the reduction in fat mass, intra-abdominal WAT depots of $Nrf2^{-/-}$ mice showed smaller unilocular adipocytes compared with wild type mice (Fig. 1*E*). The frequency of smaller fat cells, quantitated from H&E images, was significantly higher in $Nrf2^{-/-}$ WAT (Fig. 1*F*). In addition, BAT from $Nrf2^{-/-}$ mice showed smaller multilocular lipid droplets (Fig. 1*G*). However, strain differences in subcutaneous adipocytes were not observed (data not shown).

$Nrf2^{-/-}$ Mice on a High Fat Diet Showed Improved Metabolic Profiles—$Nrf2^{-/-}$ mice on a high fat diet exhibited decreased fasting glucose levels compared with wild type controls (Fig. 2*A*). Glucose tolerance tests showed significantly lower blood glucose levels in $Nrf2^{-/-}$ mice at the 90 and 120 min time points (Fig. 2*B*). The area under the curve $(AUC)_{0-120\ \mathrm{min}}$ of blood glucose was also significantly lower in $Nrf2^{-/-}$ mice than that in wild type controls (Fig. 2*C*). The improvement in glucose tolerance in $Nrf2^{-/-}$ mice is not due to increased insulin secretion because plasma insulin levels were lower in $Nrf2^{-/-}$ mice compared with wild type controls (Fig. 2*D*). In addition, serum triglyceride levels were also lower in $Nrf2^{-/-}$ mice (Fig. 2*E*). Taken together, these findings suggest that *Nrf2* deficiency provides protection against the deleterious effects of a high fat diet on plasma levels of glucose and triglycerides.

$Nrf2^{-/-}$ Mice on High Fat Diet Demonstrate Increased Energy Expenditure—Potential mechanisms, including reduced food intake or increased energy expenditure, could contribute to reduced adiposity in $Nrf2^{-/-}$ mice. To investigate this possibility, we monitored the food consumption and metabolic activities using the Comprehensive Laboratory Animal Monitoring System. Food intake per body weight in $Nrf2^{-/-}$ mice was comparable with that of wild type mice fed the same diet (Fig. 3*A*). The activity of mice was also measured for 72 h under a 12-h light-dark cycle. No significant difference was observed in either horizontal activity or rearing behavior between $Nrf2^{-/-}$ and wild type mice (Fig. 3*B*). Although energy expenditure levels in wild type and $Nrf2^{-/-}$ mice fed a regular diet were similar (data not shown), O_2 consumption and CO_2 generation were significantly higher in $Nrf2^{-/-}$ mice compared with wild type controls under high fat feeding (Fig. 3, *C* and *D*). Respiratory quotient (*RER*) levels were identical in $Nrf2^{-/-}$ and wild type mice, indicating that the utilization of carbohydrate and fat was similar for both groups (Fig. 3*E*). This suggests that despite the increase in metabolic activity, $Nrf2^{-/-}$ mice have not shifted their energy source dramatically. These findings suggest

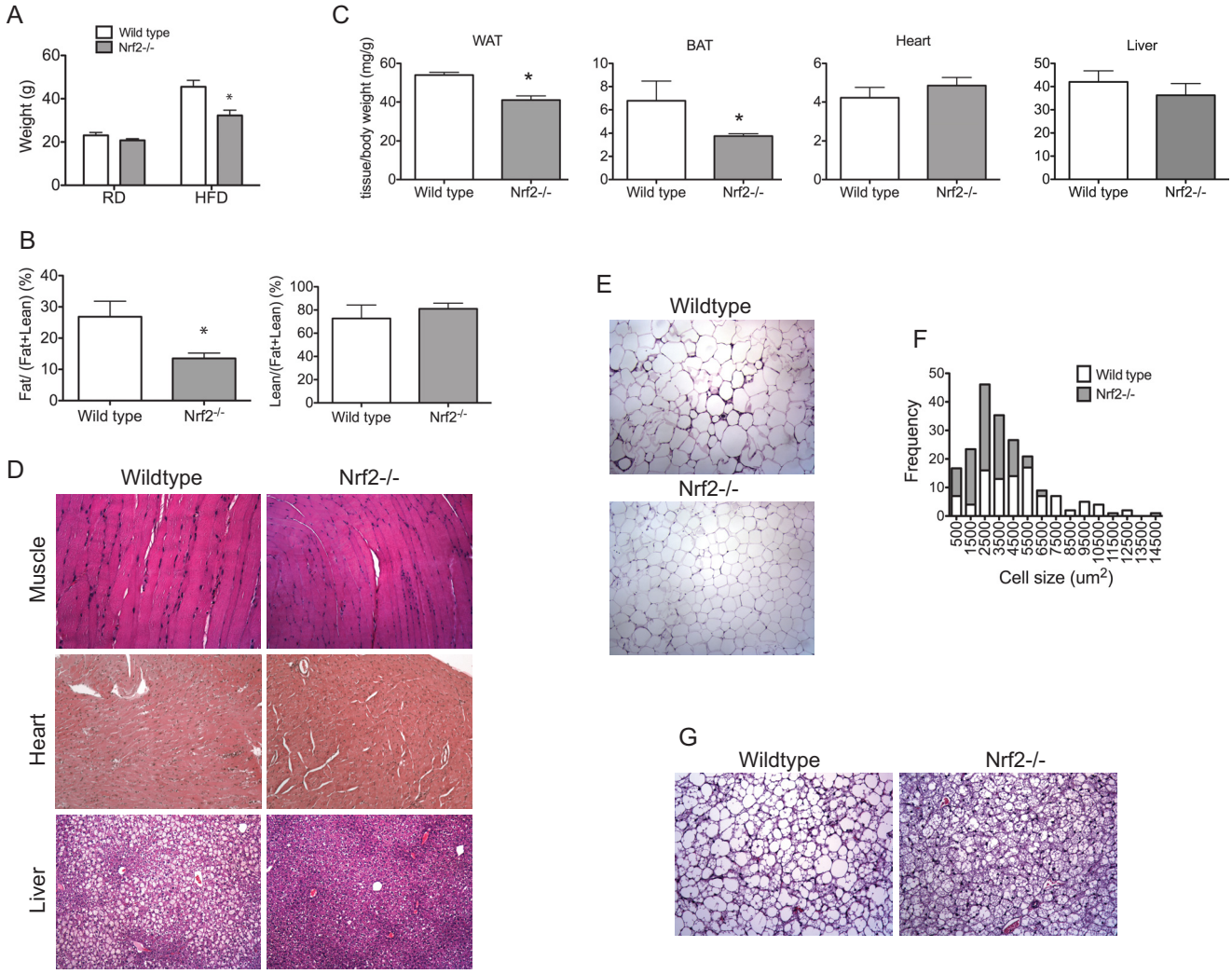

FIGURE 1. ***Nrf2*$^{-/-}$ mice are resistant to high fat diet-induced obesity.** *A*, comparison of body weights of wild type and *Nrf2*$^{-/-}$ mice on a regular diet (*RD*) and after 6 weeks of high fat diet (*HFD*). *B*, echo MRI analysis of body compositions of wild type and *Nrf2*$^{-/-}$ mice. *C*, comparison of WAT, BAT, and liver and heart weights, normalized to body weights, of wild type and *Nrf2*$^{-/-}$ mice after 6 weeks of high fat diet. Shown are representative histological sections of skeletal muscle, heart, liver (*D*), and peritoneal fat from wild type and *Nrf2*$^{-/-}$ mice (*E*). *F*, histogram depicting the size distribution of the measured white adipocytes in wild type and *Nrf2*$^{-/-}$ mice. *G*, representative interscapular brown fat from wild type and *Nrf2*$^{-/-}$ mice. All tissues are taken from mice after 6 weeks of high fat diet feeding. *Error bars*, S.E.

that resistance to obesity of *Nrf2*$^{-/-}$ mice is due to increased energy expenditure by increasing metabolic rate.

Nrf2-deficient WAT Show Increased Oxygen Consumption—To further substantiate these findings, we investigated whether loss of *Nrf2* affects mitochondrial function by comparing OCRs of adipose tissues from wild type and *Nrf2*$^{-/-}$ mice. WAT isolated from *Nrf2*$^{-/-}$ mice fed either a normal or high fat diet showed an increase in basal OCR in comparison with wild type (Fig. 4*A*). Proton leak-dependent respiration measured in the presence of the ATP synthase inhibitor, oligomycin, was significantly higher in WAT of *Nrf2*$^{-/-}$ mice fed a normal diet and was further increased in *Nrf2*$^{-/-}$ mice fed a high fat diet (Fig. 4*B*), suggesting that mitochondrial coupling was diminished. High fat diet feeding led to an increase in maximal and reserve mitochondrial respiratory capacities in both wild type and *Nrf2*$^{-/-}$ mice, but no difference was seen between the genotypes (Fig. 4, *C* and *D*). Although WAT of *Nrf2*$^{-/-}$ mice showed a decrease in reserve capacity, this difference did not reach statistical significance (Fig. 4*D*). Taken together, these results suggest that mitochondrial activity is increased in *Nrf2*$^{-/-}$ adipocytes and that this increase in activity is potentially caused by increased proton leak across the mitochondrial inner membrane.

Nrf2-deficient MEF Cells Show Increased Oxygen Consumption—To determine whether increased cellular respiration is intrinsic to *Nrf2* deficiency, we measured OCR in MEFs utilizing the XF24 extracellular flux analyzer. Compared with wild type MEF cells, basal oxygen consumption rates in *Nrf2*$^{-/-}$ MEF cells were increased 2.5-fold (Fig. 5*A*). To confirm these results, oxygen utilization of wild type and *Nrf2*$^{-/-}$ MEFs was also compared using oxygen biosensor plates in which the fluorescent signal from oxygen-sensitive dye is quenched by O_2. In this assay, *Nrf2*$^{-/-}$ MEF cells showed a similar increase in oxygen consumption compared with wild type MEFs (Fig. 5*B*). To demonstrate that this effect is specific to *Nrf2* deficiency, we asked if re-expression of *Nrf2* would lower the oxygen consumption rates in *Nrf2*$^{-/-}$ MEF cells. As shown in Fig. 5*C*, retrovirus-mediated expression of *Nrf2* in *Nrf2*$^{-/-}$ MEF cells decreased oxygen consumption by >50%.

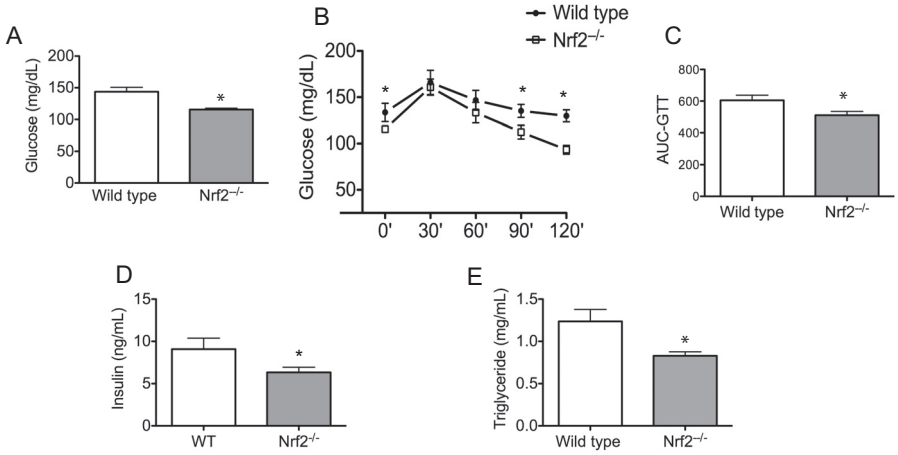

FIGURE 2. ***Nrf2*$^{-/-}$ mice on a high fat diet showed improved metabolic profiles.** *A*, fasting glucose levels in wild type and *Nrf2*$^{-/-}$ mice. *B*, glucose tolerance test. Mice starved for 12 h were given an intraperitoneal injection of glucose (1 mg/g body weight). Blood samples were taken at the times indicated from the tail vein of the same animals. Glucose was measured as indicated under "Experimental Procedures." *C*, area under the curve (*AUC*) of blood glucose levels during intraperitoneal glucose tolerance test. Shown are plasma insulin (*D*) and triglyceride levels (*E*) of wild type and *Nrf2*$^{-/-}$ mice. Experiments were performed after 6 weeks of high fat diet feeding in all groups. Data are expressed as means ± S.E. (*error bars*) ($n = 8$ mice/group), and significance was determined by Student's *t* test (*, $p < 0.05$).

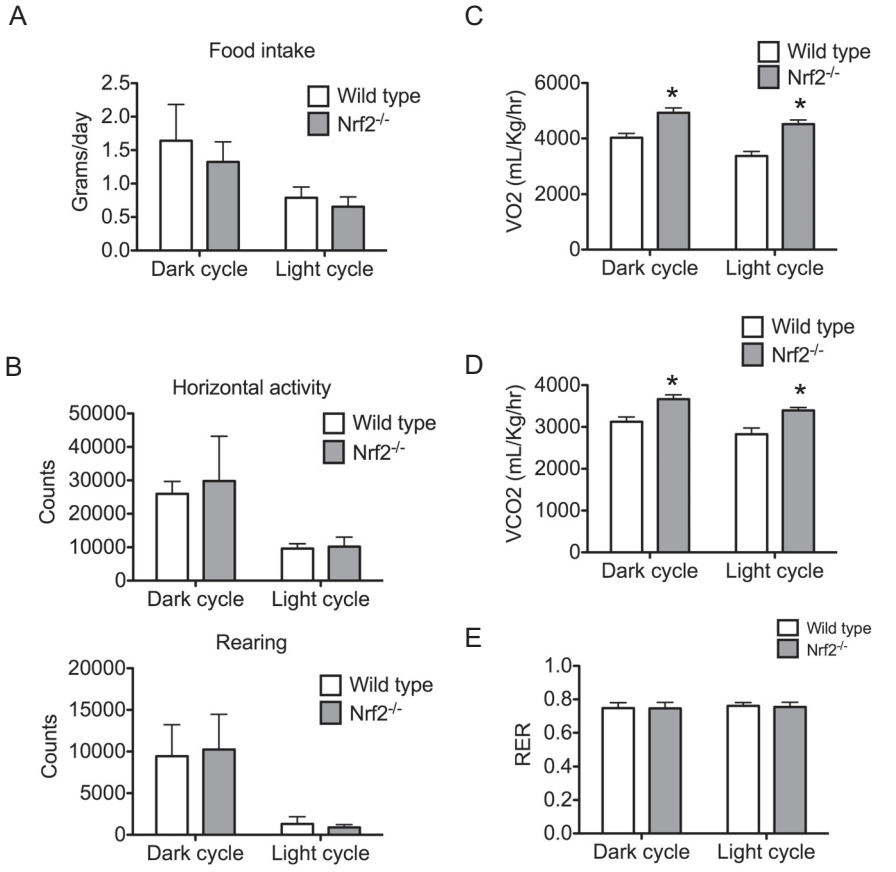

FIGURE 3. ***Nrf2*$^{-/-}$ mice on high fat diet demonstrate increased energy expenditure.** *A*, daily food intake of wild type and *Nrf2*$^{-/-}$ mice over a 6-day period. *B*, physical activity of wild type and *Nrf2*$^{-/-}$ mice over a 3-day period measured by horizontal activity and rearing light beam breaks using the Comprehensive Laboratory Animal Monitoring System. Counts of horizontal activity and rearing are shown for both dark and light cycles. Wild type and *Nrf2*$^{-/-}$ mice were analyzed for oxygen consumption (*VO2*) (*C*), energy expenditure (*D*), and respiratory exchange ratio (*E*) determined by the Comprehensive Laboratory Animal Monitoring System over a 3-day period. Values from dark and light cycles are shown. Experiments were performed after 6 weeks of high fat diet feeding in all groups. Data are expressed as means ± S.E. (*error bars*) ($n = 6$ mice/group), and significance was determined by Student's *t* test (*, $p < 0.05$).

Brown Fat Markers Are Up-regulated in White Adipose Tissues of Nrf2$^{-/-}$ *Mice*—To determine the molecular basis of the lean phenotype of *Nrf2*$^{-/-}$ mice, we performed gene expression analysis by high throughput RNA-seq of adipocytes derived from intra-abdominal fat pads of wild type and *Nrf2* mice fed a high fat diet. Genes that were differentially expressed

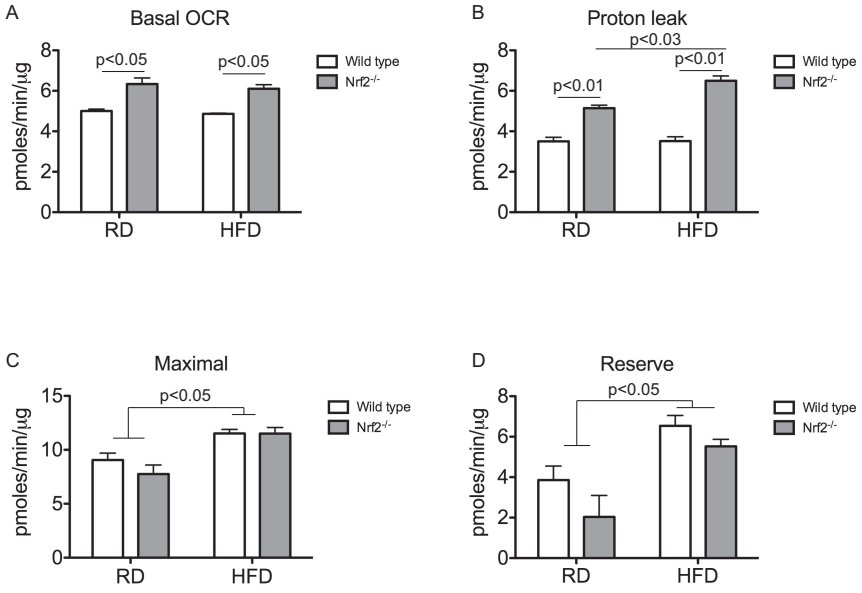

FIGURE 4. ***Nrf2*-deficient WAT show increased oxygen consumption.** *A–D*, quantitation of basal OCR (*A*), proton leak (oligomycin OCR − rotenone/antimycin OCR) (*B*), maximal rate (FCCP OCR − rotenone/antimycin OCR) (*C*), and reserve capacity (rotenone/antimycin OCR) (*D*) in WAT of wild type and *Nrf2*$^{-/-}$ mice. Data were normalized to total protein and represented as means ± S.E. (*error bars*) (n = 3/group). Significance was determined by two-way ANOVA and Bonferroni post hoc comparison. *HFD*, high fat diet; *RD*, regular diet.

were analyzed with Ingenuity Pathway Analysis software. The top biological functions and disease networks identified by IPA in *Nrf2*$^{-/-}$ included cell signaling, small molecule biochemistry, lipid metabolism, cancer, and cell death (Fig. 6*A*). Overall, the top ranked networks were significantly enriched for pathways involved in lipid metabolism. Of the genes identified in these pathways, *Nrf2*$^{-/-}$ white adipose tissue showed increased expression of *Ucp1* and other brown adipocyte markers. UCP1 functions as an uncoupler of mitochondrial ATP production, and its up-regulation might account for the change in energetics in *Nrf2*$^{-/-}$ mice. Hence, we focused our attention on these genes to validate the RNA-seq data. Quantitative RT-PCR analysis showed significant up-regulation of *Ucp1*, *Cox7a1*, *Cox8b*, *Sirt3*, *CideA*, *Pgc1a*, *Tfam*, and *Nrf1* (nuclear respiratory factor 1) in WAT of *Nrf2*$^{-/-}$ mice fed a high fat diet (Fig. 6*B*). Interestingly, expression of some of these genes associated with brown fat was also up-regulated in *Nrf2*$^{-/-}$ WAT under regular diet conditions (Fig. 6*B*). Western blotting analysis showed increased UCP1 protein expression in *Nrf2*$^{-/-}$ WAT that was further enhanced by high fat diet (Fig. 6, *C–E*). Unlike WAT, expression of *Ucp1* and other brown fat markers was not altered significantly in *Nrf2*$^{-/-}$ brown adipose tissues under regular diet or high fat diet conditions (data not shown). Taken together, these data suggest that WAT in *Nrf2*$^{-/-}$ mice gained some BAT-like features.

Oxidative Stress Modulates Oxygen Consumption and UCP1 Expression—Nrf2 plays a pivotal role in oxidative stress response. Hence, we sought to determine whether elevated oxygen consumption rates in *Nrf2*-deficient cells are potentially linked to oxidative stress. To confirm oxidative stress in our model, we assessed glutathione status in adipose tissues of wild type and *Nrf2*$^{-/-}$ mice. WAT from *Nrf2*$^{-/-}$ mice fed a high fat diet showed a decrease in GSH with a corresponding increase in GSSG, leading to a reduction in GSH/GSSG ratio (Fig. 7, *A–C*). A decreased GSH/GSSG ratio is indicative of oxidative stress. To further test the effects of oxidative stress on cellular respiration, we compared oxygen consumption rates in MEF cells derived from wild type and *Nrf2*-deficient mice. Oxygen consumption rates were 2-fold higher in *Nrf2*$^{-/-}$ cells compared with wild type (Fig. 7*D*). Wild type cells treated with glucose oxidase to induce oxidative stress also showed a 2-fold increase in oxygen consumption (Fig. 7*D*). However, glucose oxidase treatment did not lead to further enhancement of oxygen consumption in *Nrf2*$^{-/-}$ cells. As expected, elevated intracellular reactive oxygen species levels were detected in *Nrf2*$^{-/-}$ cells and wild type cells treated with glucose oxidase (Fig. 7*E*). We then examined the effects of BHA, a free radical scavenging antioxidant, on oxygen consumption in *Nrf2*$^{-/-}$ cells. As shown in Fig. 7*D*, oxygen consumption in *Nrf2*$^{-/-}$ cells was reduced by BHA treatment. BHA treatment had no effect in wild type cells. Next, we examined the effects of oxidative stress on UCP1 expression. Wild type MEF cells treated with glucose oxidase led to a marked induction of *Ucp1* mRNA and protein (Fig. 7, *F* and *G*). Consistent with the effects of oxidative stress, *Nrf2*$^{-/-}$ MEF cells showed increased *Ucp1* mRNA and protein compared with wild type cells (Fig. 7, *H* and *I*), and treatment with antioxidants (*N*-acetylcysteine, a free radical scavenging compound, or MnTBAP, a cell-permeable superoxide dismutase mimetic) led to a decrease in *Ucp1* in *Nrf2*$^{-/-}$ MEF cells (Fig. 7*J*). To test the involvement of *Ucp1* in cellular oxygen consumption, we used SB203580, a p38 MAPK inhibitor known to suppress Ucp1 expression (46). SB203580 treatment resulted in a dose-dependent decrease in OCR in *Nrf2*$^{-/-}$ MEF cells (Fig. 7*K*). Taken together, these data suggest that *Nrf2* deficiency in MEFs results in oxidative stress, which in turn up-regulates Ucp1 expression and cellular respiration.

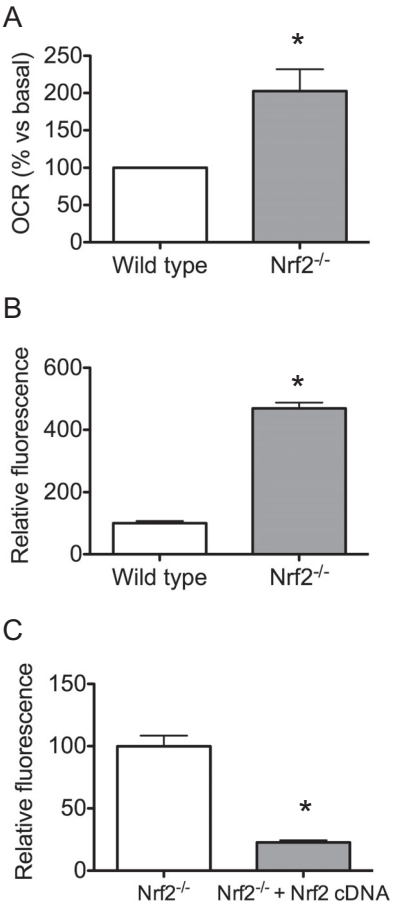

FIGURE 5. ***Nrf2*-deficient MEF cells show increased oxygen consumption.** *A*, Seahorse X-24 analysis of basal OCR normalized to total protein in wild type and $Nrf2^{-/-}$ MEF cells. Data represent means ± S.E. ($n = 3$/group), and significance was determined by Student's *t* test (*, $p < 0.05$). *B*, oxygen consumption of wild type and $Nrf2^{-/-}$ MEF cells; *C*, $Nrf2^{-/-}$ and $Nrf2^{-/-}$ MEF cells stably expressing *Nrf2* cDNA. Quantitative changes in respiratory rate were calculated from oxygen consumption curves measured using BD Oxygen Biosensor plates. Data represent means of maximum fluorescence intensity normalized to cell number ± S.E. (*error bars*) of 3–4 independent experiments.

Discussion

Obesity and its related disorders are leading causes of morbidity and mortality worldwide. Various treatment modalities for obesity have been met with limited success. Hence, identification of novel targets that can potentially be employed for prevention and treatment of obesity is of great interest. In this study, we have demonstrated that loss of *Nrf2* protects mice from diet-induced obesity. $Nrf2^{-/-}$ mice exhibit increased energy expenditure and brown adipose-like changes in white adipose depots. Loss of *Nrf2* in cells results in increased oxygen consumption and expression of UCP1, and we have shown that oxidative stress can modulate UCP1 expression and oxygen consumption in cells. Taken together, these results suggest that increased uncoupled respiration due to increased oxidative stress brought on by the loss of *Nrf2* helps to contribute to the lean phenotype of $Nrf2^{-/-}$ animals fed a high fat diet.

Nrf2 plays an important role in oxidative stress response by regulating the basal and inducible expression of a large battery of antioxidant genes. It is interesting to note that a deficiency in various *Nrf2* target genes leads to a similar decrease in adiposity and improved metabolic parameters. Knock-outs of *Gclm* and *Gpx1*, which are genes involved in antioxidant defense and glutathione synthesis, result in mice with decreased adipose tissue mass and with protection from high fat diet-induced obesity. In addition, these mice show increased energy expenditure, decreased serum insulin levels, and increased insulin sensitivity (47, 48). Conversely, it has been shown that transgenic mice overexpressing *Gpx1* are insulin-resistant and obese (49). Another pathway of potential interest involves thioredoxins, which are cellular antioxidants that protect against oxidative stress by promoting the reduction of other proteins via a cysteine thiol-disulfide exchange reaction. Thioredoxins are kept in the reduced state via TXNRD1 (thioredoxin reductase 1). TXNIP (thioredoxin-interacting protein), on the other hand, can increase reactive oxygen species by inhibiting TXNRD1. It has been demonstrated that *Nrf2* suppresses *Txnip* gene expression. Thus, loss of *Nrf2* results in increased *Txnip* expression and a subsequent increase in oxidative stress (50). Interestingly, *Txnip* knock-out mice also demonstrate increased adiposity when exposed to high fat diet feeding (51). Whereas findings suggest that the lean phenotype in $Nrf2^{-/-}$ mice is linked to antioxidant dysfunction and oxidative stress, *Nrf2* affects the expression of many genes besides just those involved in oxidative stress, and it is possible that multiple mechanisms are contributing to the ability of *Nrf2* knock-out to attenuate diet-induced weight gain and accumulation of body fat. Additionally, our model represents a whole animal knock-out of *Nrf2*. The possibility that *Nrf2* deficiency in non-adipose tissue may contribute to the observed phenotype will require further experimentation using adipose tissue-specific knock-out models of *Nrf2* deficiency.

UCP1 uncouples the proton motive force generated in the mitochondria from ATP production to produce heat, and UCP1 has been shown to play an important role in energy homeostasis and obesity. Mice deficient in *Ucp1* are shown to be susceptible to weight gain, whereas overexpression of *Ucp1* provides protection against diet-induced obesity (16, 17). UCP2 and UCP3, which are homologs of UCP1, also have uncoupling function in the mitochondria and serve as potential targets for increased metabolic capacity. *Ucp2* is ubiquitously expressed at low levels throughout the body, whereas *Ucp3* is limited to skeletal and cardiac muscle (52, 53). Mice overexpressing *Ucp3* in muscle are lean and have increased energy metabolism as well as decreased levels of serum glucose (54). Additionally, polymorphisms in the *Ucp2* gene have been associated with obesity and decreased metabolic rates in humans (55–57). In this study, we found that $Nrf2^{-/-}$ mice fed a high fat diet have an elevated metabolic rate in both whole animals and isolated white adipose tissue that is associated with an up-regulation of *Ucp1* in their abdominal white adipose depots. Similarly, the basal oxygen consumption rate in *Nrf2*-deficient cells is increased, and *Ucp1* expression is induced. However, up-regulation of *Ucp2* and *Ucp3* expression was not observed in *Nrf2*-deficient fat tissues (data not shown). Additionally, we observed decreased levels of *Ucp3* in muscle tissues of $Nrf2^{-/-}$ mice (data not shown) that are consistent with data demonstrating direct regulation of *Ucp3* by *Nrf2* (58). Thus, UCP2 and UCP3 do not appear to provide additional mitochondrial uncoupling in the

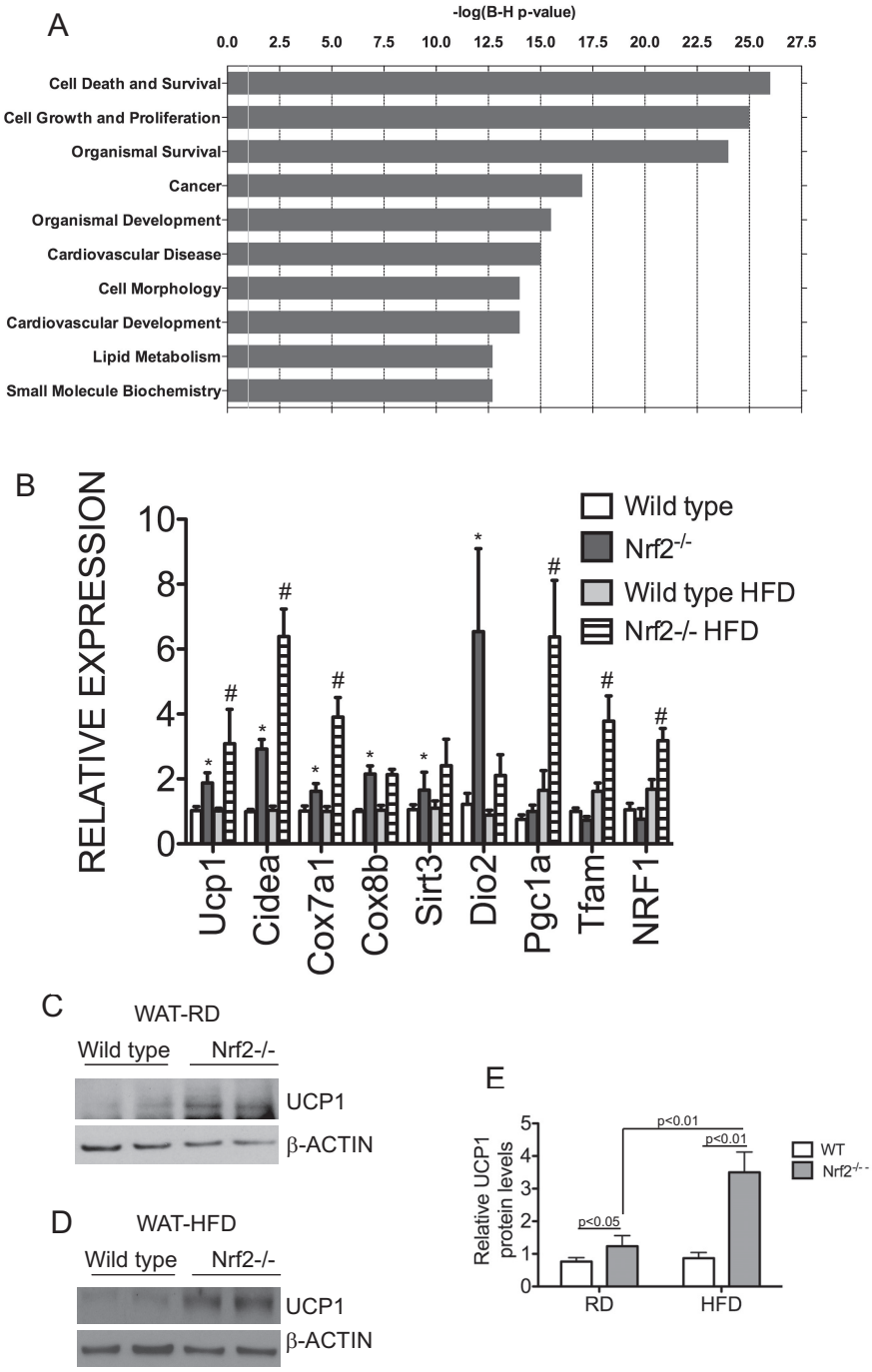

FIGURE 6. **Brown fat markers are up-regulated in white adipose tissues of *Nrf2*$^{-/-}$ mice.** *A*, Ingenuity Pathway Analysis of differentially expressed genes in wild type and *Nrf2*$^{-/-}$ white adipose tissues. Genes that were significantly different between wild type and *Nrf2*$^{-/-}$ white adipose tissues were used as input for pathway analysis. The top 10 overrepresented canonical pathways of up-regulated genes found in *Nrf2*$^{-/-}$ white adipose tissues compared with controls are shown. Category names are presented on the *y* axis. The *x* axis indicates the $-\log(p)$ value of the overrepresentation analysis. *B*, quantitative RT-PCR analysis of brown fat markers in abdominal white adipose tissues of wild type and *Nrf2*$^{-/-}$ mice fed a high fat diet (*HFD*) or regular diet (*RD*). Expression levels were quantitated relative to *Rplpo* levels as an internal reference and calculated as $2^{(Ct\ \text{test gene} - Ct\text{RPLP0})}$. Bar graphs depict mean values ± S.E. (*error bars*) of 4–6 different samples of each genotype, and significance was assessed by two-way ANOVA and post-hoc Bonferroni analysis. *, significance between wild type and *Nrf2*$^{-/-}$ regular diet samples; #, significance between regular diet and high fat diet samples. *C–E*, Western blotting analysis of UCP1 protein levels in abdominal white adipose tissues of wild type and *Nrf2*$^{-/-}$ mice fed a high fat or regular diet, respectively. β-Actin levels were used as a loading control. *E*, bar graph shows quantitation of protein levels; significance was assessed by two-way ANOVA and post hoc Bonferroni analysis.

adipose tissue of *Nrf2* knock-out animals. These findings suggest that UCP1-dependent thermogenesis is a mechanism by which energy expenditure in *Nrf2*$^{-/-}$ mice is up-regulated.

Whereas a wide range of stimuli, including cold exposure, diet, and exercise, controls *Ucp1* expression (15, 59), these factors are not likely to play a role here because mice in this study were housed and maintained in a controlled environment, and both wild type and *Nrf2*$^{-/-}$ mice showed similar food intake and physical activity. In addition, expression of Rip140 and Lxr, both of which are negative regulators of *Ucp1* expression (60–

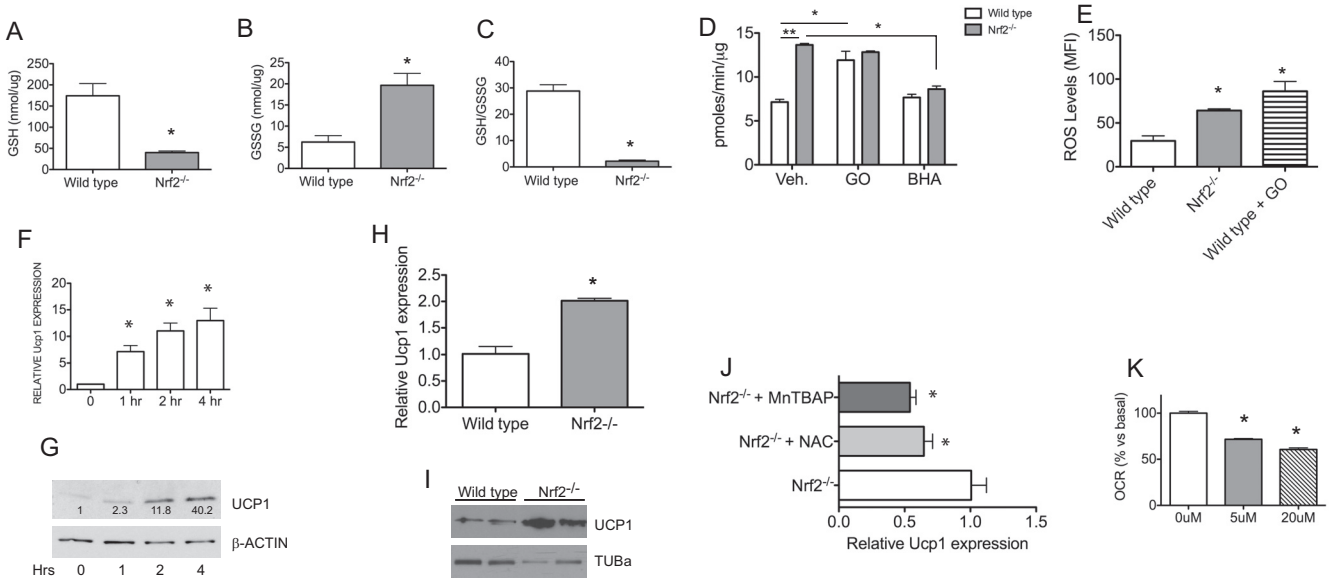

FIGURE 7. **Oxidative stress modulates oxygen consumption and UCP1 expression.** *A–C*, GSH (*A*), GSSG (*B*), and GSH/GSSG levels (*C*) of WAT from wild type and *Nrf2*$^{-/-}$ mice after 6 weeks of high fat diet feeding. Data represent means ($n = 3$/group) ± S.E. (*error bars*); *, $p < 0.05$. *D*, Seahorse X-24 analysis of basal oxygen consumption rate in wild type and *Nrf2*$^{-/-}$ MEF cells with and without treatment with glucose oxidase or BHA. Data were normalized to total protein and are represented as means ± S.E. ($n = 6$/group). Significance was assessed by two-way ANOVA and post hoc Bonferroni analysis. *, $p < 0.05$; **, $p < 0.001$. *E*, dichlorodihydrofluorescein fluorescence levels in wild type, *Nrf2*$^{-/-}$, and wild type cells treated with glucose oxidase. Data represent means ($n = 3/4$/group) ± S.E.; *, $p < 0.05$. *F*, expression of *Ucp1* mRNA in wild type MEF cells treated with glucose oxidase to induce oxidative stress for the indicated times. *G*, Western blotting analysis of UCP1 protein in wild type MEF cells treated with glucose oxidase for the indicated times. Densitometric quantitations of band intensities are shown. *H*, basal expression of *Ucp1* mRNA levels in wild type and *Nrf2*$^{-/-}$ MEF cells. Results represent means ($n = 3$/group) ± S.E.; *, $p < 0.05$. *I*, Western blotting analysis of basal UCP1 protein in wild type and *Nrf2*$^{-/-}$ MEF cells. *J*, expression of Ucp1 mRNA levels in *Nrf2*$^{-/-}$ MEF cells treated with *N*-acetylcysteine (*NAC*) or MnTBAP. Bar graphs represent mean values ± S.E. ($n = 3$); *, $p < 0.05$. *K*, Seahorse X-24 analysis of basal OCR in *Nrf2*$^{-/-}$ MEF cells treated with SB203580. Data represent means ± S.E. ($n = 3$/group), and significance was determined by Student's *t* test (*, $p < 0.05$).

62), was not altered in *Nrf2*$^{-/-}$ adipose tissues (data not shown). Expression of *Ucp1* is activated by oxidative stress (46, 63, 64). Consistent with this, we show that glucose oxidase-induced oxidative stress in MEF cells up-regulates *Ucp1* expression, and antioxidant treatment down-regulates *Ucp1* expression in *Nrf2*$^{-/-}$ MEF cells. We also found that Pgc1a expression is increased in WAT of Nrf2$^{-/-}$ mice fed a high fat diet, which is known to exacerbate oxidative stress in fat cells (65). It has been shown that oxidative stress increases the expression of *Pgc1a*, and PGC1a interacts with other nuclear hormone receptors in white adipose cells to enhance mitochondrial biogenesis and the expression of *Ucp1* (64, 66, 67). Hence, we surmise that acquisition of brown fat features by WAT depots in *Nrf2*$^{-/-}$ mice is driven in part by oxidative stress induction of *Pgc1a* expression.

Data obtained previously showed that *Nrf2*$^{-/-}$ mice of C57/129 mixed genetic background are resistant to high fat diet-induced obesity (41). In agreement with this, our results also show that *Nrf2*$^{-/-}$ mice derived on a C57/BL/6 background are resistant to diet-induced obesity. Here we demonstrated that *Nrf2*$^{-/-}$ mice have increased energy expenditure and acquisition of brown fat-like gene expression in their WAT depots. There is growing evidence that the acquisition of brown-like fat cells in WAT protects against both genetic and diet-induced obesity through increased metabolic activity, and this "browning" phenomenon has become a subject of considerable interest for possible treatment of obesity and metabolic syndrome (68–70). Browning of WAT has been shown to occur in mouse models of prolactin receptor deficiency, IkB kinase ϵ deficiency, COXII overexpression, and increased prostaglandin synthesis (71–74). In these instances, mice displayed a protection against diet-induced obesity as well as increased oxygen consumption. Additionally, FGF21 has been shown to exert anti-obesogenic effects and ameliorates insulin and leptin resistance in ob/ob mice (75). It has been shown that mice lacking *Nrf2* demonstrate protection against diet-induced obesity, maintain insulin sensitivity, and demonstrate increased circulating levels of FGF21 and expression of *Fgf21* in liver and WAT (76). However, no difference in *Fgf21* expression was found between wild type and *Nrf2*-deficient white adipose tissue or liver in our experiments (data not shown). The basis of this discrepant result is not known currently; however, our high fat diet duration of 6 weeks was significantly shorter than the 180 days tested in the above study. We propose that the metabolic and gene expression changes observed in our *Nrf2*$^{-/-}$ model are due in part to increased levels of oxidative stress, caused by a combination of decreased antioxidant capacity through the loss of *Nrf2* function and the additional oxidative stress provided through exposure to a high fat diet. Currently, we cannot rule out the possibility that increased UCP1 expression in *Nrf2*$^{-/-}$ mice is through modulation of downstream target genes, independent of oxidative stress effects. Previous data have shown that deficiency of *Nrf2* results in down-regulation of *Pparγ* (75). *Pparγ* knock-out mice demonstrate decreased adipose tissue mass, protection against diet-induced obesity, and increased expression of *Ucp1* in white adipose tissue (77, 78). It is thought that decreased PPARγ activity drives increased expression of prostaglandin E synthase, which, in concert with COXII, drives

the formation of prostaglandin, which is hypothesized to be important in the formation of brown adipose tissue within white adipose tissue depots (77). It is likely that the phenotype observed in *Nrf2*$^{-/-}$ mice is due to a complex interplay of a variety of pathways.

Further supporting this complex role of *Nrf2*, recent studies have shown that overexpression of *Nrf2* through the use of graded knockdown of *Keap1* actually provides protection against the onset of diabetes in genetic models of diabetes in mice (79). This suggests a beneficial role for *Nrf2* in the protection against the development of diabetes with increased expression of *Nrf2* resulting in decreased blood glucose and protection against obesity in a db/db mouse background. However, it is worth noting that in addition to the protective effects of *Nrf2*, the same group also found that mice lacking *Nrf2* demonstrate decreased serum glucose levels compared with control mice, which correlates with data from our model of *Nrf2* deficiency. In mice doubly deficient in *Keap1* and leptin, there was a resistance to high fat diet-induced obesity and a decrease in adipose tissue weight that was also associated with impaired insulin signaling, hyperglycemia, and glucose intolerance (80). Additional studies utilizing the ob/ob genetic model of obesity have yielded varied results. *Nrf2* knock-out animals crossed into the ob/ob mouse background, using either a whole animal or fat-specific *Nrf2* knock-out, demonstrated that loss of *Nrf2* resulted in decreased adipose tissue mass yet aggravated insulin resistance, hyperglycemia, and hypertriglyceridemia (81). This seems to demonstrate that in genetic models of obesity and diabetes, the results of *Nrf2* modulation can vary drastically, depending on the specific conditions of the model. In order to most closely compare results with our own, it is important to look at systems similar to ours, in which the experiments are performed looking at strictly diet-induced models of obesity rather than genetic models of obesity and diabetes. For example, *Keap1* knockdown mice in the C57BL/6 background without crossing to any genetic models of obesity or diabetes gained significantly more weight than wild type animals as well as developed glucose intolerance, increased inflammation, and hepatic steatosis when placed on a high fat diet (82). As mentioned previously, other groups have also shown that *Nrf2* knock-out mice were found to be resistant to long term high fat diet-induced obesity (68). These results coincide with our data and seem to suggest that increased *Nrf2* levels lead to increased obesity and that *Nrf2* deficiency may provide protective benefits in a diet-induced obesity model. These varied results in the literature suggest a complex interaction between *Nrf2*, obesity, and diabetes, and further research will probably provide insight.

In summary, *Nrf2*-deficient mice are protected from diet-induced obesity and exhibit increased energy expenditure associated with the up-regulation of brown adipose tissue-specific genes in white adipose depots. Cell-based experiments demonstrated that increased UCP1 expression is associated with increased cellular oxidative stress. These observations suggest a promising model for increasing energy expenditure in white adipose tissue through *Nrf2* and the possibility of pharmacological modulation of *Nrf2* or regulation of oxidative stress as treatments for obesity and its related disorders.

Author Contributions—J. Y. C. and T. W. K. conceived and wrote the paper. K. S. coordinated the studies and performed the studies in Figs. 1–7 and also wrote the paper. M. V. analyzed the experiments shown in Fig. 6*A*. B. G. helped to design and provided technical assistance in experiments shown in Figs. 4 and 5. J. N., J. V., and B. G. provided technical assistance and contributed to the preparation of figures. All authors reviewed the results and approved the final version of the manuscript.

References

1. Lowell, B. B., and Spiegelman, B. M. (2000) Towards a molecular understanding of adaptive thermogenesis. *Nature* **404,** 652–660
2. Tseng, Y. H., Cypess, A. M., and Kahn, C. R. (2010) Cellular bioenergetics as a target for obesity therapy. *Nat. Rev. Drug Discov.* **9,** 465–482
3. Cohade, C., Osman, M., Pannu, H. K., and Wahl, R. L. (2003) Uptake in supraclavicular area fat ("U.S.A.-Fat"): description on 18F-FDG PET/CT. *J. Nucl. Med.* **44,** 170–176
4. Enerbäck, S. (2010) Human brown adipose tissue. *Cell metabolism* **11,** 248–252
5. Ravussin, E., and Galgani, J. E. (2011) The implication of brown adipose tissue for humans. *Annu. Rev. Nutr.* **31,** 33–47
6. Cypess, A. M., Lehman, S., Williams, G., Tal, I., Rodman, D., Goldfine, A. B., Kuo, F. C., Palmer, E. L., Tseng, Y. H., Doria, A., Kolodny, G. M., and Kahn, C. R. (2009) Identification and importance of brown adipose tissue in adult humans. *N. Engl. J. Med.* **360,** 1509–1517
7. Nedergaard, J., Bengtsson, T., and Cannon, B. (2007) Unexpected evidence for active brown adipose tissue in adult humans. *Am. J. Physiol. Endocrinol. Metab.* **293,** E444–E452
8. Saito, M., Okamatsu-Ogura, Y., Matsushita, M., Watanabe, K., Yoneshiro, T., Nio-Kobayashi, J., Iwanaga, T., Miyagawa, M., Kameya, T., Nakada, K., Kawai, Y., and Tsujisaki, M. (2009) High incidence of metabolically active brown adipose tissue in healthy adult humans: effects of cold exposure and adiposity. *Diabetes* **58,** 1526–1531
9. van Marken Lichtenbelt, W. D., Vanhommerig, J. W., Smulders, N. M., Drossaerts, J. M., Kemerink, G. J., Bouvy, N. D., Schrauwen, P., and Teule, G. J. (2009) Cold-activated brown adipose tissue in healthy men. *N. Engl. J. Med.* **360,** 1500–1508
10. Virtanen, K. A., Lidell, M. E., Orava, J., Heglind, M., Westergren, R., Niemi, T., Taittonen, M., Laine, J., Savisto, N. J., Enerbäck, S., and Nuutila, P. (2009) Functional brown adipose tissue in healthy adults. *N. Engl. J. Med.* **360,** 1518–1525
11. Zingaretti, M. C., Crosta, F., Vitali, A., Guerrieri, M., Frontini, A., Cannon, B., Nedergaard, J., and Cinti, S. (2009) The presence of UCP1 demonstrates that metabolically active adipose tissue in the neck of adult humans truly represents brown adipose tissue. *FASEB J.* **23,** 3113–3120
12. Porter, R. K., and Brand, M. D. (1995) Causes of differences in respiration rate of hepatocytes from mammals of different body mass. *Am. J. Physiol.* **269,** R1213–1224
13. Rolfe, D. F., Newman, J. M., Buckingham, J. A., Clark, M. G., and Brand, M. D. (1999) Contribution of mitochondrial proton leak to respiration rate in working skeletal muscle and liver and to SMR. *Am. J. Physiol.* **276,** C692–C699
14. Rothwell, N. J., and Stock, M. J. (1983) Luxuskonsumption, diet-induced thermogenesis and brown fat: the case in favour. *Clin. Sci.* **64,** 19–23
15. Feldmann, H. M., Golozoubova, V., Cannon, B., and Nedergaard, J. (2009) UCP1 ablation induces obesity and abolishes diet-induced thermogenesis in mice exempt from thermal stress by living at thermoneutrality. *Cell Metab.* **9,** 203–209
16. Kopecky, J., Clarke, G., Enerbäck, S., Spiegelman, B., and Kozak, L. P. (1995) Expression of the mitochondrial uncoupling protein gene from the aP2 gene promoter prevents genetic obesity. *J. Clin. Invest.* **96,** 2914–2923
17. Li, B., Nolte, L. A., Ju, J. S., Han, D. H., Coleman, T., Holloszy, J. O., and Semenkovich, C. F. (2000) Skeletal muscle respiratory uncoupling prevents diet-induced obesity and insulin resistance in mice. *Nat. Med.* **6,** 1115–1120

18. Barbatelli, G., Murano, I., Madsen, L., Hao, Q., Jimenez, M., Kristiansen, K., Giacobino, J. P., De Matteis, R., and Cinti, S. (2010) The emergence of cold-induced brown adipocytes in mouse white fat depots is determined predominantly by white to brown adipocyte transdifferentiation. *Am. J. Physiol. Endocrinol. Metab.* **298,** E1244–E1253
19. Bartelt, A., and Heeren, J. (2014) Adipose tissue browning and metabolic health. *Nat. Rev. Endocrinol.* **10,** 24–36
20. Kozak, L. P. (2011) The genetics of brown adipocyte induction in white fat depots. *Front. Endocrinol.* **2,** 64
21. Petrovic, N., Walden, T. B., Shabalina, I. G., Timmons, J. A., Cannon, B., and Nedergaard, J. (2010) Chronic peroxisome proliferator-activated receptor gamma (PPARγ) activation of epididymally derived white adipocyte cultures reveals a population of thermogenically competent, UCP1-containing adipocytes molecularly distinct from classic brown adipocytes. *J. Biol. Chem.* **285,** 7153–7164
22. Biswas, M., and Chan, J. Y. (2010) Role of Nrf1 in antioxidant response element-mediated gene expression and beyond. *Toxicol. Appl. Pharmacol.* **244,** 16–20
23. Kobayashi, A., Ito, E., Toki, T., Kogame, K., Takahashi, S., Igarashi, K., Hayashi, N., and Yamamoto, M. (1999) Molecular cloning and functional characterization of a new Cap 'n' collar family transcription factor Nrf3. *J. Biol. Chem.* **274,** 6443–6452
24. Motohashi, H., and Yamamoto, M. (2004) Nrf2-Keap1 defines a physiologically important stress response mechanism. *Trends Mol. Med.* **10,** 549–557
25. Itoh, K., Wakabayashi, N., Katoh, Y., Ishii, T., O'Connor, T., and Yamamoto, M. (2003) Keap1 regulates both cytoplasmic-nuclear shuttling and degradation of Nrf2 in response to electrophiles. *Genes Cells* **8,** 379–391
26. Wakabayashi, N., Dinkova-Kostova, A. T., Holtzclaw, W. D., Kang, M. I., Kobayashi, A., Yamamoto, M., Kensler, T. W., and Talalay, P. (2004) Protection against electrophile and oxidant stress by induction of the phase 2 response: fate of cysteines of the Keap1 sensor modified by inducers. *Proc. Natl. Acad. Sci. U.S.A.* **101,** 2040–2045
27. Giudice, A., and Montella, M. (2006) Activation of the Nrf2-ARE signaling pathway: a promising strategy in cancer prevention. *Bioessays* **28,** 169–181
28. Kwak, M. K., Wakabayashi, N., Itoh, K., Motohashi, H., Yamamoto, M., and Kensler, T. W. (2003) Modulation of gene expression by cancer chemopreventive dithiolethiones through the Keap1-Nrf2 pathway. Identification of novel gene clusters for cell survival. *J. Biol. Chem.* **278,** 8135–8145
29. Nguyen, T., Sherratt, P. J., and Pickett, C. B. (2003) Regulatory mechanisms controlling gene expression mediated by the antioxidant response element. *Annu. Rev. Pharmacol. Toxicol.* **43,** 233–260
30. Osburn, W. O., and Kensler, T. W. (2008) Nrf2 signaling: an adaptive response pathway for protection against environmental toxic insults. *Mutat. Res.* **659,** 31–39
31. Kobayashi, M., and Yamamoto, M. (2006) Nrf2-Keap1 regulation of cellular defense mechanisms against electrophiles and reactive oxygen species. *Adv. Enzyme Regul.* **46,** 113–140
32. Wang, L., He, X., Szklarz, G. D., Bi, Y., Rojanasakul, Y., and Ma, Q. (2013) The aryl hydrocarbon receptor interacts with nuclear factor erythroid 2-related factor 2 to mediate induction of NAD(P)H:quinoneoxidoreductase 1 by 2,3,7,8-tetrachlorodibenzo-*p*-dioxin. *Arch. Biochem. Biophys.* **537,** 31–38
33. Lu, S. C. (2009) Regulation of glutathione synthesis. *Mol. Aspects Med.* **30,** 42–59
34. Chan, K., Han, X. D., and Kan, Y. W. (2001) An important function of Nrf2 in combating oxidative stress: detoxification of acetaminophen. *Proc. Natl. Acad. Sci. U.S.A.* **98,** 4611–4616
35. He, X., Chen, M. G., and Ma, Q. (2008) Activation of Nrf2 in defense against cadmium-induced oxidative stress. *Chem. Res. Toxicol.* **21,** 1375–1383
36. He, X., Lin, G. X., Chen, M. G., Zhang, J. X., and Ma, Q. (2007) Protection against chromium (VI)-induced oxidative stress and apoptosis by Nrf2. Recruiting Nrf2 into the nucleus and disrupting the nuclear Nrf2/Keap1 association. *Toxicol. Sci.* **98,** 298–309
37. Ma, Q., Battelli, L., and Hubbs, A. F. (2006) Multiorgan autoimmune inflammation, enhanced lymphoproliferation, and impaired homeostasis of reactive oxygen species in mice lacking the antioxidant-activated transcription factor Nrf2. *Am. J. Pathol.* **168,** 1960–1974
38. Ramos-Gomez, M., Kwak, M. K., Dolan, P. M., Itoh, K., Yamamoto, M., Talalay, P., and Kensler, T. W. (2001) Sensitivity to carcinogenesis is increased and chemoprotective efficacy of enzyme inducers is lost in nrf2 transcription factor-deficient mice. *Proc. Natl. Acad. Sci. U.S.A.* **98,** 3410–3415
39. Lee, J. M., Li, J., Johnson, D. A., Stein, T. D., Kraft, A. D., Calkins, M. J., Jakel, R. J., and Johnson, J. A. (2005) Nrf2, a multi-organ protector? *FASEB J.* **19,** 1061–1066
40. Hou, Y., Xue, P., Bai, Y., Liu, D., Woods, C. G., Yarborough, K., Fu, J., Zhang, Q., Sun, G., Collins, S., Chan, J. Y., Yamamoto, M., Andersen, M. E., and Pi, J. (2012) Nuclear factor erythroid-derived factor 2-related factor 2 regulates transcription of CCAAT/enhancer-binding protein β during adipogenesis. *Free Radic. Biol. Med.* **52,** 462–472
41. Pi, J., Leung, L., Xue, P., Wang, W., Hou, Y., Liu, D., Yehuda-Shnaidman, E., Lee, C., Lau, J., Kurtz, T. W., and Chan, J. Y. (2010) Deficiency in the nuclear factor E2-related factor-2 transcription factor results in impaired adipogenesis and protects against diet-induced obesity. *J. Biol. Chem.* **285,** 9292–9300
42. Chan, K., Lu, R., Chang, J. C., and Kan, Y. W. (1996) NRF2, a member of the NFE2 family of transcription factors, is not essential for murine erythropoiesis, growth, and development. *Proc. Natl. Acad. Sci. U.S.A.* **93,** 13943–13948
43. Dunham-Snary, K. J., Sandel, M. W., Westbrook, D. G., and Ballinger, S. W. (2014) A method for assessing mitochondrial bioenergetics in whole white adipose tissues. *Redox Biol.* **2,** 656–660
44. Rolo, A. P., Palmeira, C. M., and Cortopassi, G. A. (2009) Biosensor plates detect mitochondrial physiological regulators and mutations in vivo. *Anal. Biochem.* **385,** 176–178
45. Kemp, M., Go, Y. M., and Jones, D. P. (2008) Nonequilibrium thermodynamics of thiol/disulfide redox systems: a perspective on redox systems biology. *Free Radic. Biol. Med.* **44,** 921–937
46. Ro, S. H., Nam, M., Jang, I., Park, H. W., Park, H., Semple, I. A., Kim, M., Kim, J. S., Park, H., Einat, P., Damari, G., Golikov, M., Feinstein, E., and Lee, J. H. (2014) Sestrin2 inhibits uncoupling protein 1 expression through suppressing reactive oxygen species. *Proc. Natl. Acad. Sci. U.S.A.* **111,** 7849–7854
47. Kendig, E. L., Chen, Y., Krishan, M., Johansson, E., Schneider, S. N., Genter, M. B., Nebert, D. W., and Shertzer, H. G. (2011) Lipid metabolism and body composition in Gclm(−/−) mice. *Toxicol. Appl. Pharmacol.* **257,** 338–348
48. Loh, K., Deng, H., Fukushima, A., Cai, X., Boivin, B., Galic, S., Bruce, C., Shields, B. J., Skiba, B., Ooms, L. M., Stepto, N., Wu, B., Mitchell, C. A., Tonks, N. K., Watt, M. J., *et al.* (2009) Reactive oxygen species enhance insulin sensitivity. *Cell Metab.* **10,** 260–272
49. McClung, J. P., Roneker, C. A., Mu, W., Lisk, D. J., Langlais, P., Liu, F., and Lei, X. G. (2004) Development of insulin resistance and obesity in mice overexpressing cellular glutathione peroxidase. *Proc. Natl. Acad. Sci. U.S.A.* **101,** 8852–8857
50. He, X., and Ma, Q. (2012) Redox regulation by nuclear factor erythroid 2-related factor 2: gatekeeping for the basal and diabetes-induced expression of thioredoxin-interacting protein. *Mol. Pharmacol.* **82,** 887–897
51. Chutkow, W. A., Birkenfeld, A. L., Brown, J. D., Lee, H. Y., Frederick, D. W., Yoshioka, J., Patwari, P., Kursawe, R., Cushman, S. W., Plutzky, J., Shulman, G. I., Samuel, V. T., and Lee, R. T. (2010) Deletion of the α-arrestin protein Txnip in mice promotes adiposity and adipogenesis while preserving insulin sensitivity. *Diabetes* **59,** 1424–1434
52. Boss, O., Samec, S., Paoloni-Giacobino, A., Rossier, C., Dulloo, A., Seydoux, J., Muzzin, P., and Giacobino, J. P. (1997) Uncoupling protein-3: a new member of the mitochondrial carrier family with tissue-specific expression. *FEBS Lett.* **408,** 39–42
53. Fleury, C., Neverova, M., Collins, S., Raimbault, S., Champigny, O., Levi-Meyrueis, C., Bouillaud, F., Seldin, M. F., Surwit, R. S., Ricquier, D., and Warden, C. H. (1997) Uncoupling protein-2: a novel gene linked to obesity and hyperinsulinemia. *Nat. Genet.* **15,** 269–272

54. Clapham, J. C., Arch, J. R., Chapman, H., Haynes, A., Lister, C., Moore, G. B., Piercy, V., Carter, S. A., Lehner, I., Smith, S. A., Beeley, L. J., Godden, R. J., Herrity, N., Skehel, M., Changani, K. K., *et al.* (2000) Mice overexpressing human uncoupling protein-3 in skeletal muscle are hyperphagic and lean. *Nature* **406,** 415–418
55. Mahadik, S. R., Lele, R. D., Saranath, D., Seth, A., and Parikh, V. (2012) Uncoupling protein-2 (UCP2) gene expression in subcutaneous and omental adipose tissue of Asian Indians: relationship to adiponectin and parameters of metabolic syndrome. *Adipocyte* **1,** 101–107
56. Mexitalia, M., Yamauchi, T., Utari, A., Sjarif, D. R., Subagio, H. W., Soemantri, A., and Ishida, T. (2013) The role of uncoupling protein 2 and 3 genes polymorphism and energy expenditure in obese Indonesian children. *J. Pediatr. Endocrinol. Metab.* **26,** 441–447
57. Qian, L., Xu, K., Xu, X., Gu, R., Liu, X., Shan, S., and Yang, T. (2013) UCP2–866G/A, Ala55Val and UCP3–55C/T polymorphisms in association with obesity susceptibility: a meta-analysis study. *PLoS One* **8,** e58939
58. Anedda, A., López-Bernardo, E., Acosta-Iborra, B., Saadeh Suleiman, M., Landázuri, M. O., and Cadenas, S. (2013) The transcription factor Nrf2 promotes survival by enhancing the expression of uncoupling protein 3 under conditions of oxidative stress. *Free Radic. Biol. Med.* **61,** 395–407
59. Ringholm, S., Grunnet Knudsen, J., Leick, L., Lundgaard, A., Munk Nielsen, M., and Pilegaard, H. (2013) PGC-1α is required for exercise- and exercise training-induced UCP1 up-regulation in mouse white adipose tissue. *PLoS One* **8,** e64123
60. Christian, M., Kiskinis, E., Debevec, D., Leonardsson, G., White, R., and Parker, M. G. (2005) RIP140-targeted repression of gene expression in adipocytes. *Mol. Cell. Biol.* **25,** 9383–9391
61. Leonardsson, G., Steel, J. H., Christian, M., Pocock, V., Milligan, S., Bell, J., So, P. W., Medina-Gomez, G., Vidal-Puig, A., White, R., and Parker, M. G. (2004) Nuclear receptor corepressor RIP140 regulates fat accumulation. *Proc. Natl. Acad. Sci. U.S.A.* **101,** 8437–8442
62. Wang, H., Zhang, Y., Yehuda-Shnaidman, E., Medvedev, A. V., Kumar, N., Daniel, K. W., Robidoux, J., Czech, M. P., Mangelsdorf, D. J., and Collins, S. (2008) Liver X receptor α is a transcriptional repressor of the uncoupling protein 1 gene and the brown fat phenotype. *Mol. Cell. Biol.* **28,** 2187–2200
63. Echtay, K. S., Roussel, D., St-Pierre, J., Jekabsons, M. B., Cadenas, S., Stuart, J. A., Harper, J. A., Roebuck, S. J., Morrison, A., Pickering, S., Clapham, J. C., and Brand, M. D. (2002) Superoxide activates mitochondrial uncoupling proteins. *Nature* **415,** 96–99
64. Fernandez-Marcos, P. J., and Auwerx, J. (2011) Regulation of PGC-1α, a nodal regulator of mitochondrial biogenesis. *Am. J. Clin. Nutr.* **93,** 884S-890
65. Matsuzawa-Nagata, N., Takamura, T., Ando, H., Nakamura, S., Kurita, S., Misu, H., Ota, T., Yokoyama, M., Honda, M., Miyamoto, K., and Kaneko, S. (2008) Increased oxidative stress precedes the onset of high-fat diet-induced insulin resistance and obesity. *Metabolism* **57,** 1071–1077
66. St-Pierre, J., Drori, S., Uldry, M., Silvaggi, J. M., Rhee, J., Jäger, S., Handschin, C., Zheng, K., Lin, J., Yang, W., Simon, D. K., Bachoo, R., and Spiegelman, B. M. (2006) Suppression of reactive oxygen species and neurodegeneration by the PGC-1 transcriptional coactivators. *Cell* **127,** 397–408
67. Wu, Z., Puigserver, P., Andersson, U., Zhang, C., Adelmant, G., Mootha, V., Troy, A., Cinti, S., Lowell, B., Scarpulla, R. C., and Spiegelman, B. M. (1999) Mechanisms controlling mitochondrial biogenesis and respiration through the thermogenic coactivator PGC-1. *Cell* **98,** 115–124
68. Lee, P., Werner, C. D., Kebebew, E., and Celi, F. S. (2013) Functional thermogenic beige adipogenesis is inducible in human neck fat. *Int. J. Obes.* **38,** 170–176
69. Whittle, A., Relat-Pardo, J., and Vidal-Puig, A. (2013) Pharmacological strategies for targeting BAT thermogenesis. *Trends Pharmacol. Sci.* **34,** 347–355
70. Zafrir, B. (2013) Brown adipose tissue: research milestones of a potential player in human energy balance and obesity. *Horm. Metab. Res.* **45,** 774–785
71. Auffret, J., Viengchareun, S., Carré, N., Denis, R. G., Magnan, C., Marie, P. Y., Muscat, A., Fève, B., Lombès, M., and Binart, N. (2012) Beige differentiation of adipose depots in mice lacking prolactin receptor protects against high-fat-diet-induced obesity. *FASEB J.* **26,** 3728–3737
72. Chiang, S. H., Bazuine, M., Lumeng, C. N., Geletka, L. M., Mowers, J., White, N. M., Ma, J. T., Zhou, J., Qi, N., Westcott, D., Delproposto, J. B., Blackwell, T. S., Yull, F. E., and Saltiel, A. R. (2009) The protein kinase IKKϵ regulates energy balance in obese mice. *Cell* **138,** 961–975
73. Fisher, F. M., Kleiner, S., Douris, N., Fox, E. C., Mepani, R. J., Verdeguer, F., Wu, J., Kharitonenkov, A., Flier, J. S., Maratos-Flier, E., and Spiegelman, B. M. (2012) FGF21 regulates PGC-1α and browning of white adipose tissues in adaptive thermogenesis. *Genes Dev.* **26,** 271–281
74. Vegiopoulos, A., Müller-Decker, K., Strzoda, D., Schmitt, I., Chichelnitskiy, E., Ostertag, A., Berriel Diaz, M., Rozman, J., Hrabe de Angelis, M., Nüsing, R. M., Meyer, C. W., Wahli, W., Klingenspor, M., and Herzig, S. (2010) Cyclooxygenase-2 controls energy homeostasis in mice by de novo recruitment of brown adipocytes. *Science* **328,** 1158–1161
75. Kharitonenkov, A., Shiyanova, T. L., Koester, A., Ford, A. M., Micanovic, R., Galbreath, E. J., Sandusky, G. E., Hammond, L. J., Moyers, J. S., Owens, R. A., Gromada, J., Brozinick, J. T., Hawkins, E. D., Wroblewski, V. J., Li, D. S., et al. (2005) FGF-21 as a novel metabolic regulator. *J. Clin. Invest.* **115,** 1627–1635
76. Chartoumpekis, D. V., Ziros, P. G., Psyrogiannis, A. I., Papavassiliou, A. G., Kyriazopoulou, V. E., Sykiotis, G. P., and Habeos, I. G. (2011) Nrf2 represses FGF21 during long-term high-fat diet-induced obesity in mice. *Diabetes* **60,** 2465–2473
77. García-Alonso, V., López-Vicario, C., Titos, E., Morán-Salvador, E., González-Périz, A., Rius, B., Párrizas, M., Werz, O., Arroyo, V., and Clària, J. (2013) Coordinate functional regulation between microsomal prostaglandin E synthase-1 (mPGES-1) and peroxisome proliferator-activated receptor γ (PPARγ) in the conversion of white-to-brown adipocytes. *J. Biol. Chem.* **288,** 28230–28242
78. Jones, J. R., Barrick, C., Kim, K. A., Lindner, J., Blondeau, B., Fujimoto, Y., Shiota, M., Kesterson, R. A., Kahn, B. B., and Magnuson, M. A. (2005) Deletion of PPARγ in adipose tissues of mice protects against high fat diet-induced obesity and insulin resistance. *Proc. Natl. Acad. Sci. U.S.A.* **102,** 6207–6212
79. Uruno, A., Furusawa, Y., Yagishita, Y., Fukutomi, T., Muramatsu, H., Negishi, T., Sugawara, A., Kensler, T. W., and Yamamoto, M. (2013) The Keap1-Nrf2 system prevents onset of diabetes mellitus. *Mol. Cell. Biol.* **33,** 2996–3010
80. Xu, J., Kulkarni, S. R., Donepudi, A. C., More, V. R., and Slitt, A. L. (2012) Enhanced Nrf2 activity worsens insulin resistance, impairs lipid accumulation in adipose tissue, and increases hepatic steatosis in leptin-deficient mice. *Diabetes* **61,** 3208–3218
81. Xue, P., Hou, Y., Chen, Y., Yang, B., Fu, J., Zheng, H., Yarborough, K., Woods, C. G., Liu, D., Yamamoto, M., Zhang, Q., Andersen, M. E., and Pi, J. (2013) Adipose deficiency of Nrf2 in ob/ob mice results in severe metabolic syndrome. *Diabetes* **62,** 845–854
82. More, V. R., Xu, J., Shimpi, P. C., Belgrave, C., Luyendyk, J. P., Yamamoto, M., and Slitt, A. L. (2013) Keap1 knockdown increases markers of metabolic syndrome after long-term high fat diet feeding. *Free Radic. Biol. Med.* **61,** 85–94